Mineral inclusions are not immutable:
evidence of post-entrapment thermally-induced shape change of quartz in garnet

Bernardo Cesare[1]*, Matteo Parisatto[1], Lucia Mancini[2,3], Luca Peruzzo[4], Marco Franceschi[5], Tommaso Tacchetto[6], Steven Reddy[6], Richard Spiess[1], Fabrizio Nestola[1], Federica Marone[7]

Supplementary Material

Low-T Dataset:		H1-incl 1	H1-incl 2	H1-incl 3	G1-incl 1	G1-incl 2	G1-incl 3	G4-incl 1	G4-incl 2	G4-incl 3	G4-incl 4	G4-incl 5	G4-incl 6	
Sample		east. Alps	east. Alps	east. Alps	Tauern	Tauern	Tauern	Tauern	Tauern	Tauern	Tauern	Tauern	Tauern	
	unit													
Inclusion volume	μm^3	86180	73509	72911	243129	173522	161161	86611	50315	40191	11435	8806	7110	
Inclusion surface	μm^2	14292	13365	11950	46654	27936	28273	15566	14232	9399	4505	3846	2706	
Inclusion surface / volume ratio	μm^{-1}	**0,166**	**0,182**	**0,164**	**0,192**	**0,161**	**0,175**	**0,180**	**0,283**	**0,234**	**0,394**	**0,437**	**0,381**	
Equivalent sphere diameter	µm	54,80	51,97	51,83	77,44	69,20	67,52	54,89	45,80	42,50	27,95	25,62	23,86	
Surface / volume ratio of equivalent volume sphere	μm^{-1}	0,109	0,115	0,116	0,077	0,087	0,089	0,109	0,131	0,141	0,215	0,234	0,251	
High-T Dataset:		**X1-incl 1**	**X1-incl 3**	**D6-cluster**	**A2_i2**	**A2_i1**	**F6_i1**	**F6_i2**	**D7_i1**	**C1_i1**	**F2_i1**	**F2_i2**	**F2_i3**	**F2_i4**
Sample		Jubrique	Jubrique	Namibia	Jubrique	Jubrique	Athabasca	Athabasca	Namibia	Massachusetts	Athabasca	Athabasca	Athabasca	Athabasca
	unit													
Inclusion volume	μm^3	162604	219434	78009	5073	12067	179723	85167	23610	279675	159629	60597	20297	17603
Inclusion surface	μm^2	16680	20250	11000	1703	2880	17894	11242	4936	23993	16669	8560	4075	3790
Inclusion surface / volume ratio	μm^{-1}	**0,103**	**0,092**	**0,141**	**0,336**	**0,239**	**0,100**	**0,132**	**0,209**	**0,086**	**0,104**	**0,141**	**0,201**	**0,215**
Equivalent sphere diameter	µm	67,72	74,83	53,01	21,32	28,46	70,02	54,59	35,59	81,14	67,30	48,73	33,84	32,27
Surface / volume ratio of equivalent volume sphere	μm^{-1}	0,089	0,080	0,113	0,281	0,211	0,086	0,110	0,169	0,074	0,089	0,123	0,177	0,186

Table S1. Morphometric data of selected inclusions from the studied samples.

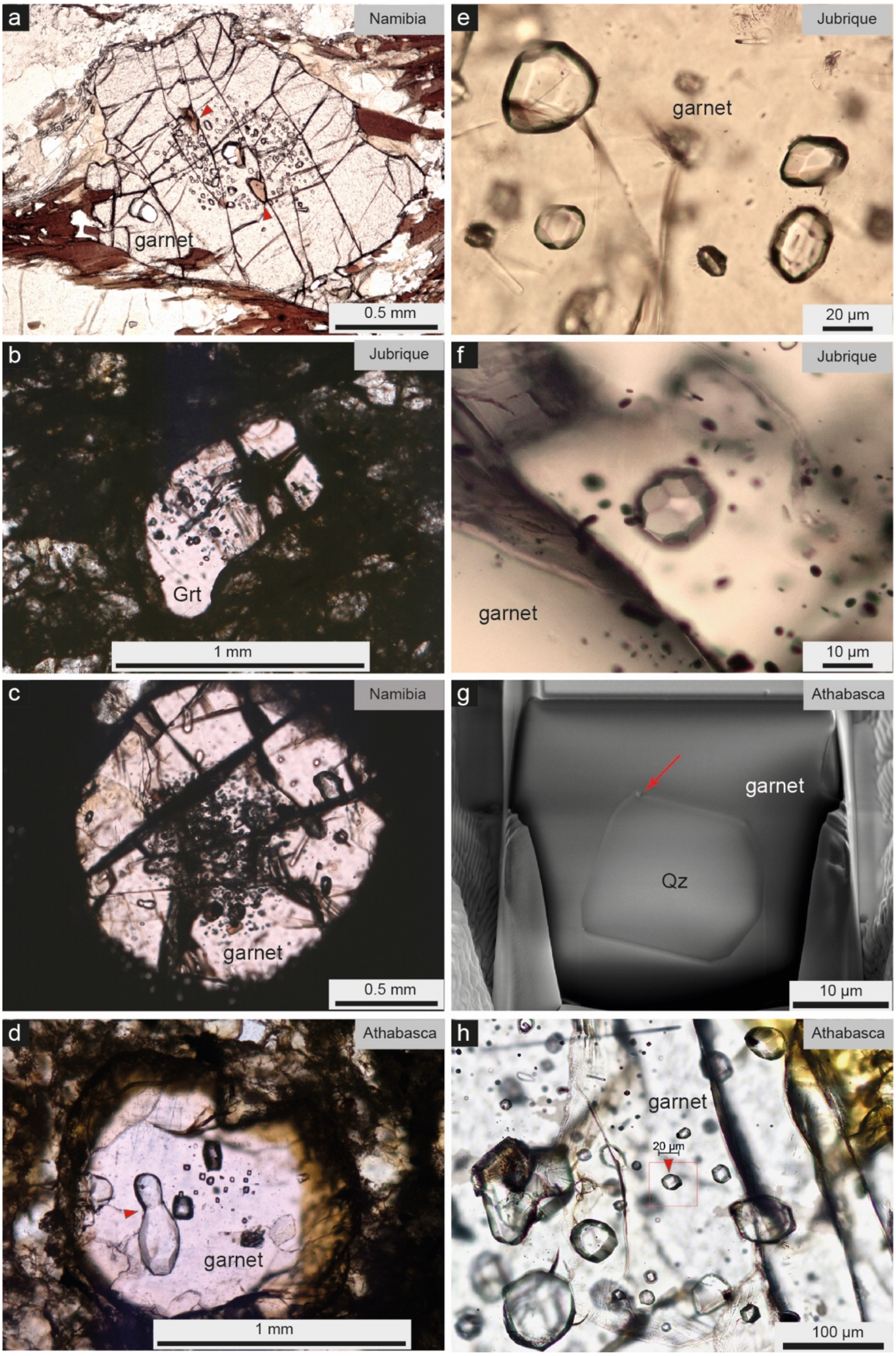

Fig. S1. Faceted quartz inclusions in garnet from granulite-facies high-T metamorphic rocks. Plane-polarized optical photomicrographs except **g**, which is a SE-BSEM image obtained during FIB serial slicing. **a-d,** views of the common microstructures shared by selected samples, with inclusions generally occurring at the cores of garnets. Arrows in **a** point to biotite inclusions; the arrow in **d** indicates two crystals of quartz joined in a composite inclusion showing features suggestive of necking down (compare Fig. $1b_4$). **e-f,** spectacular examples of quartz inclusions with negative crystal shape. Faceting can be appreciated also with optical microscopy. **g,** 2D-section obtained by FIB-SEM serial sectioning of an inclusion of quartz with well-developed straight (planar) boundaries. The arrow points to a submicrometric heavy inclusion at the interphase boundary. **h,** cluster of faceted quartz inclusions and location (arrow) of a crystal within a doubly-polished wafer of garnet used for the FIB-SEM serial sectioning.

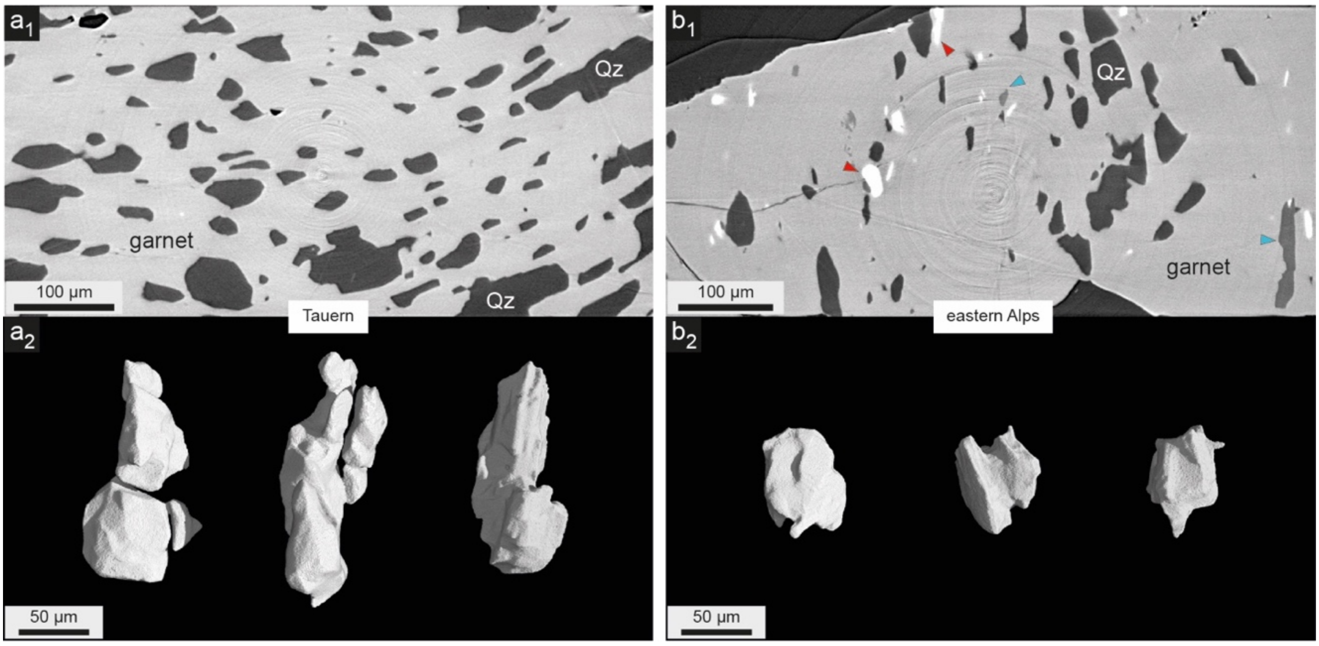

Fig. S2. **Shape of quartz inclusions in greenschist-facies low-T samples**. **a_1-b_1.** SRXTM axial slices. Blue arrows: chlorite; red arrows: ilmenite. **a_2-b_2.** 3D renderings from SRXTM data. The reconstructed slices and volumes show the highly irregular, “scalloped” shape, and the large surface/volume ratios.

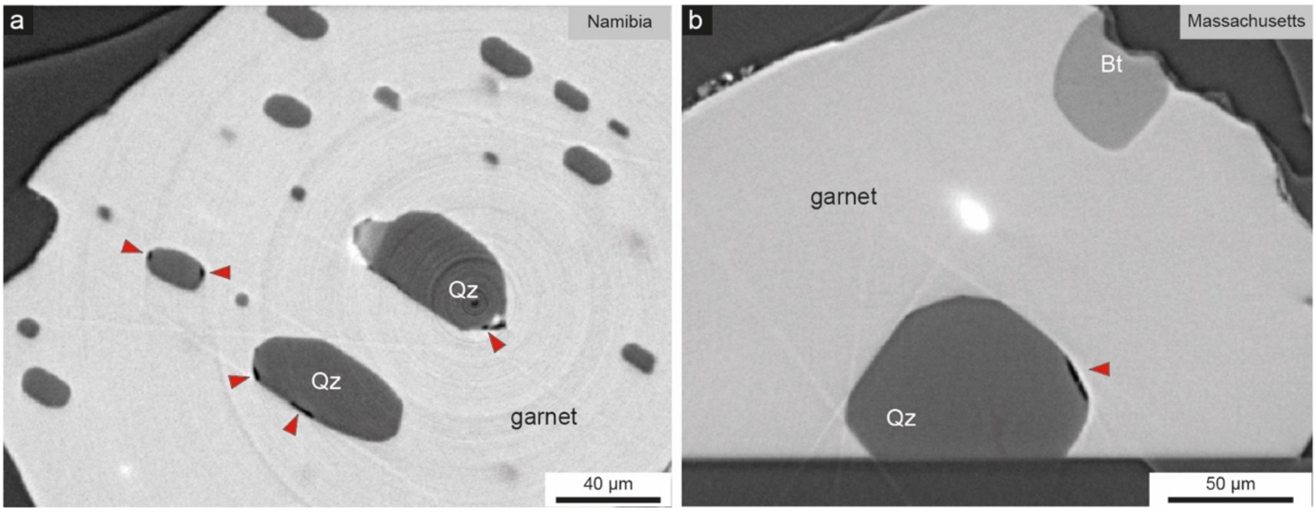

Fig. S3. **Possible pockets of fluid at interface boundaries**. **a, b,** details of SRXTM axial slices of garnet samples from Namibia and Massachusetts, respectively. **a,** along with the faceted shape, and elongation of inclusions according to an original internal foliation, some inclusions display black areas located at the boundary with garnet (red arrows). These features can be interpreted as small pockets of fluid trapped simultaneously with quartz. **b,** another example of possible fluid-coated portion of interface boundary (red arrow) in a large faceted inclusion of quartz.

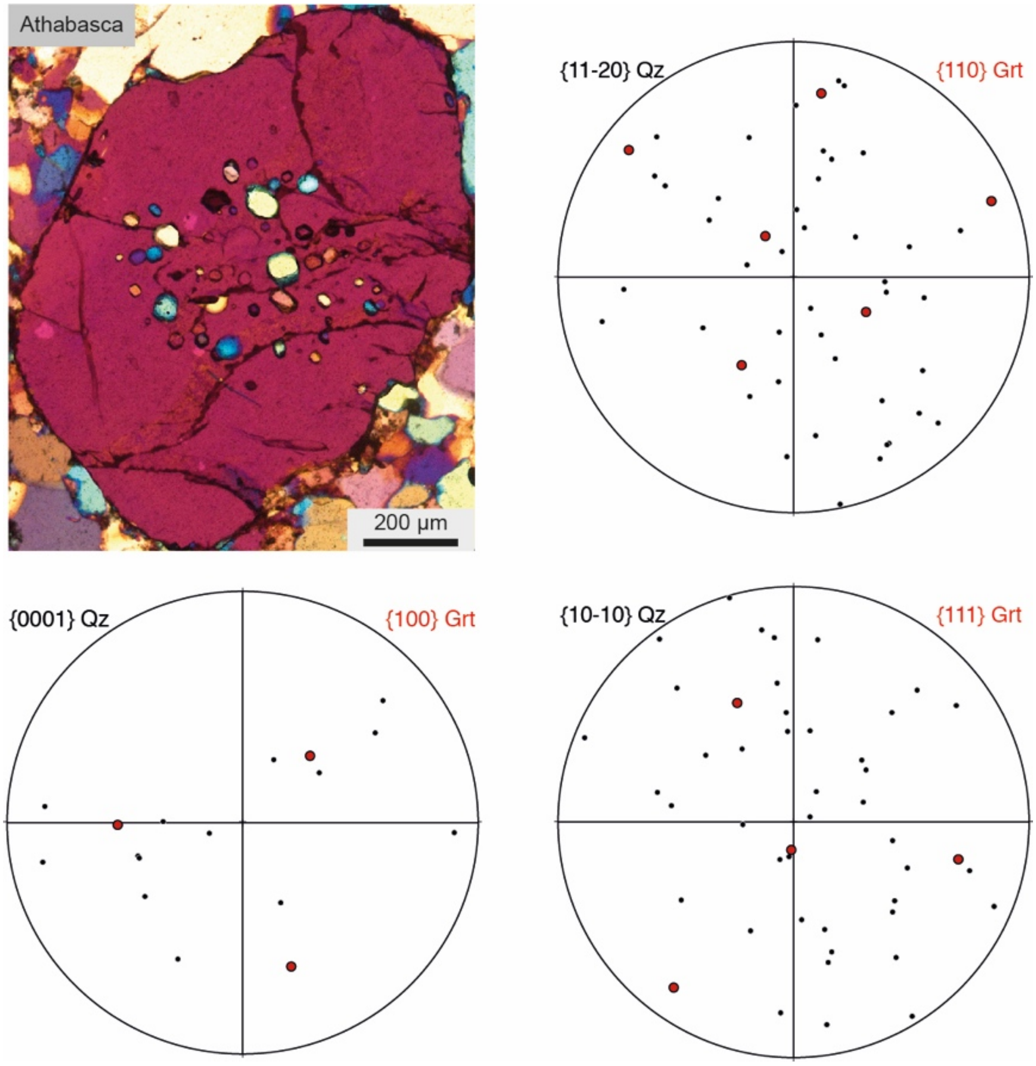

Fig. S4. **Random crystallographic orientation of quartz inclusions in granulite-facies samples**. A crossed-polarizers optical photomicrograph with lambda plate (top left) allows qualitative evaluation of the lack of preferred orientation of quartz inclusions. The three stereonets display the orientation of the main crystallographic axes of 14 inclusions of quartz (black squares) and those of the host garnet (red circles). Quartz crystals are randomly oriented with respect to one another, and therefore also with respect to the garnet.

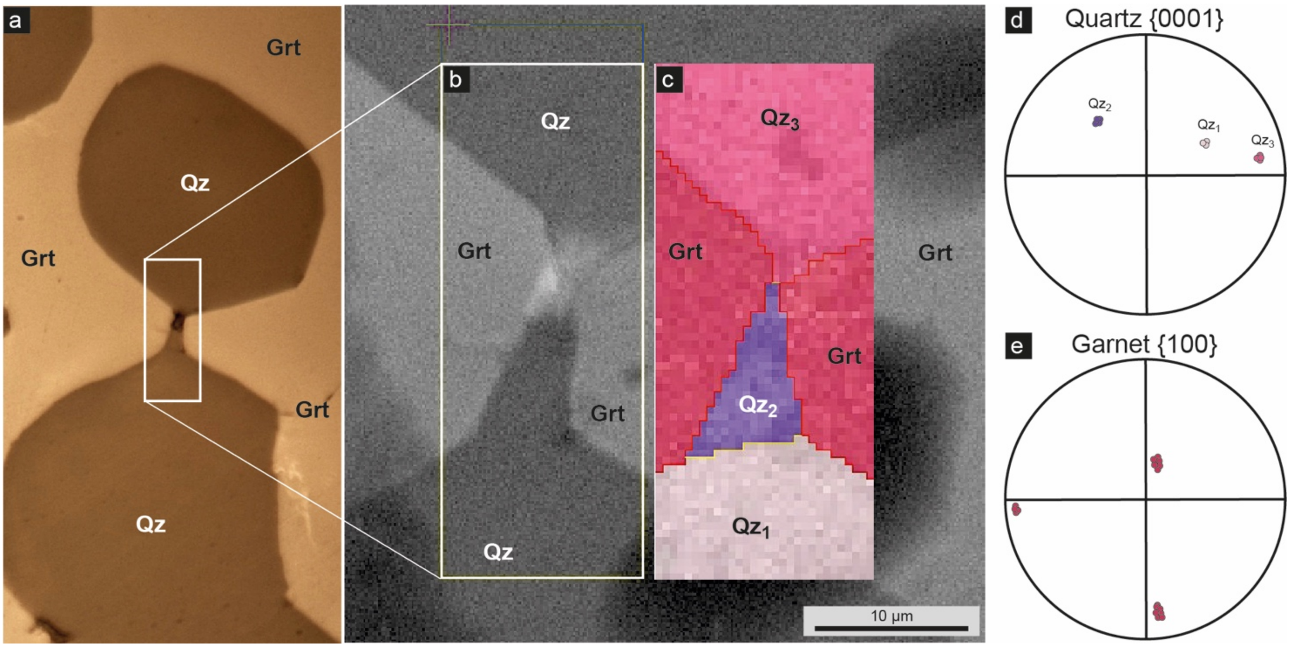

Fig. S5. Quartz neck microstructure within a garnet from a granulite-facies high-T rock sample from Swaziland. a, Reflected light photomicrograph showing the area of interest (white box) enlarged in b and c. **b, c,** Backscattered electron image and EBSD all-Euler map of the region of interest, locating three differently oriented quartz crystals: Qz_1 and Qz_3 on either side of the neck, and Qz_2 on the neck. **d, e,** equal area pole figures (lower hemisphere) displaying mismatches >50° among the {0001} orientation of the three quartz crystals, whereas {100} crystallographic directions do overlap within garnet. Step size 0.5 µm.

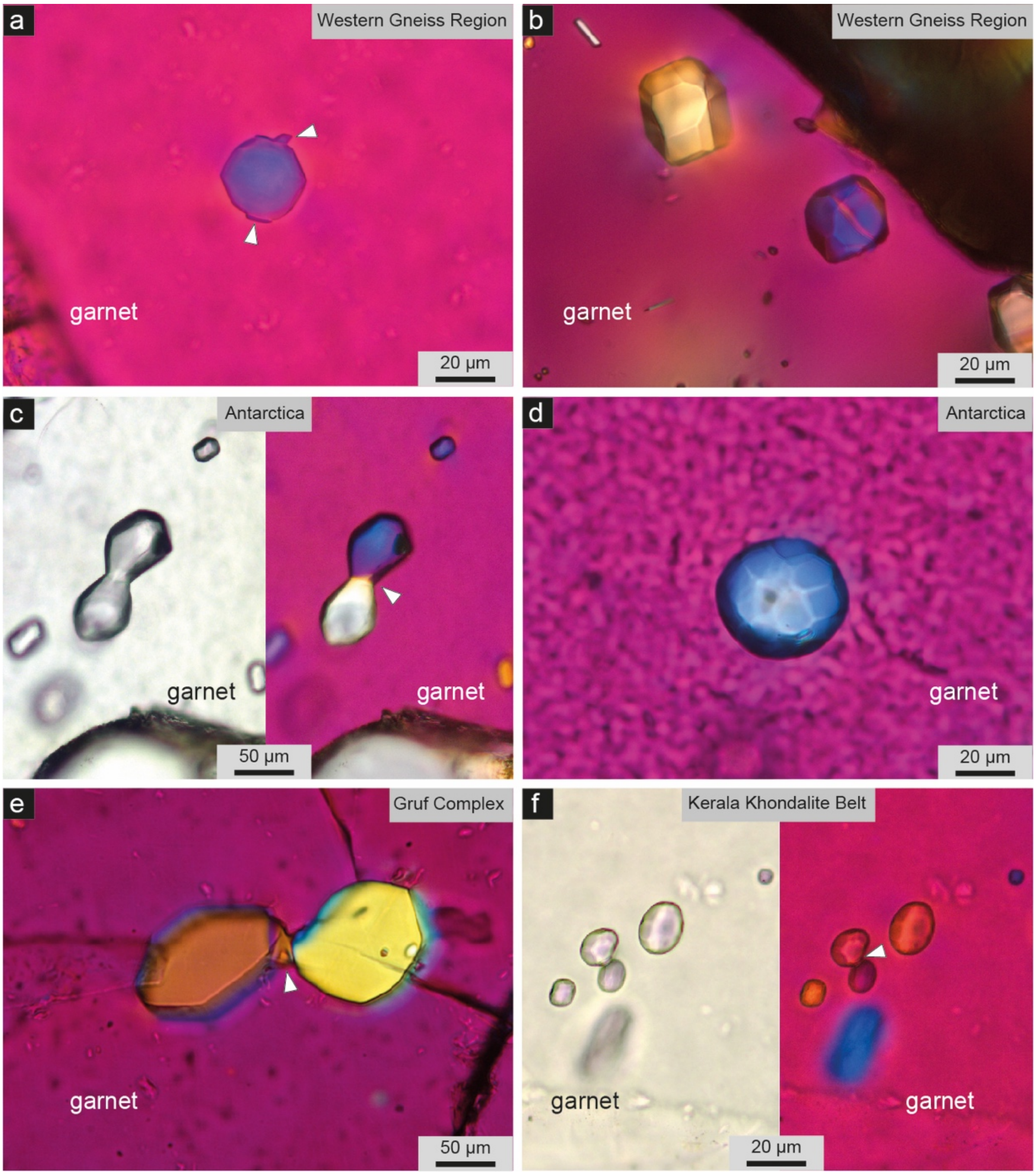

Fig. S6. Negative crystal quartz inclusions in other samples of granulite-facies high-T rocks worldwide. Crossed-polarizer optical photomicrograph with lambda plate except left parts of **c** and **f**, which are plane polarized micrographs. **a, b,** felsic granulites from near Ulsteinvik, Western Gneiss Region, Norway (sample courtesy of Bruna Carvalho). **c, d,** ultra-high-T granulites from Lützow–Holm Complex, East Antarctica (sample courtesy of Satish Kumar). **e,** ultra-high-T granulites from the Gruf Complex, italian central Alps (sample courtesy of Omar Gianola). **f,** felsic granulites from the Kerala Khondalite Belt, India. Arrows in **a** point to possible other phases at the quartz/garnet interface. Arrows in **c**, **e** and **f** indicate necking down microstructures

Supplementary Movie S1 (separate file). 3D animation obtained from SRXTM data showing a subvolume extracted from one of the Jubrique samples. By virtually removing the host garnet, one quartz internal inclusion (light blue) is revealed. The inclusion is 70 μm across and shows well-developed negative-crystal shape given by combination of facets of rhombic dodecahedron and icositetrahedron.

Supplementary Movie S2 (separate file). 3D animation obtained from SRXTM data showing a subvolume extracted from one of the Athabasca samples (approximately 340x270x300 μm^3). After virtually removing the host garnet, a cluster of faceted quartz inclusions with negative-crystal shape is highlighted (light blue), together with some heavy mineral inclusions (orange). The size of the faceted inclusion in the final part of the movie, showing well-defined rhombic dodecahedron and icositetrahedron facets, is approximately 60x50x40 μm^3.

Supplementary Movie S3 (separate file). 3D animation obtained from SRXTM data showing a subvolume extracted from one of the Swaziland samples. After virtually removing the host garnet, a composite quartz inclusion (light blue) is highlighted and isolated. The inclusion consists of three grains with partially developed negative crystal facets, joined along small necks suggesting an arrested *necking down* process.

Supplementary Movie S4 (separate file). 3D animation obtained from SRXTM data showing a subvolume extracted from one of the Tauern Window samples. After virtually removing the host garnet, a cluster of quartz inclusion (light blue) is highlighted. The inclusions are highly irregular, flattened and elongate to define an internal foliation in the sample. The surface/volume ratio of these inclusions is much larger than in high-T samples.